

AD-A154 728

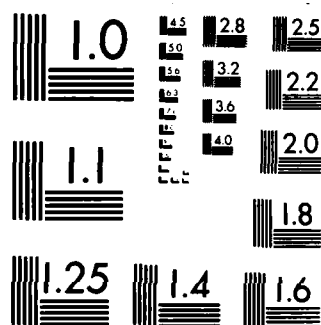
APPLICATION OF A RESISTANCE HEATER TO THE MOCVD  
(METAL-ORGANIC CHEMICAL V. (U) AEROSPACE CORP EL  
SEGUNDO CA ELECTRONICS RESEARCH LAB S I BOLDISH ET AL.  
08 MAR 85 TR-0084A(5925-01)-1 SD-TR-85-03 F/G 7/4

1/1

UNCLASSIFIED

NL





MICROCOPY RESOLUTION TEST CHART  
NATIONAL BUREAU OF STANDARDS-1963-A

②  
GR

AD-A154 728

Application of a Resistance Heater  
to the MOCVD Growth of Undoped  
and Se-Doped GaAs

S. I. BOLDISH, J. S. CIOFALO, and J. P. WENDT  
Electronics Research Laboratory  
Laboratory Operations  
The Aerospace Corporation  
El Segundo, CA 90245

8 March 1985

APPROVED FOR PUBLIC RELEASE;  
DISTRIBUTION UNLIMITED

DTIC FILE COPY

DTIC  
ELECTE  
JUN 11 1985  
S E D

Prepared for  
SPACE DIVISION  
AIR FORCE SYSTEMS COMMAND  
Los Angeles Air Force Station  
P.O. Box 92960, Worldway Postal Center  
Los Angeles, CA 90009-2960

85 5 14 003

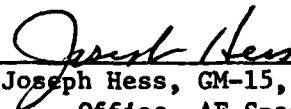
This report was submitted by The Aerospace Corporation, El Segundo, CA 90245, under Contract No. F04701-83-C-0084 with the Space Division, P.O. Box 92960, Worldway Postal Center, Los Angeles, CA 90009-2960. It was reviewed and approved for The Aerospace Corporation by D. H. Phillips, Director, Electronics Research Laboratory. Lieutenant Carl Baner, SD/CGXT, was the project officer for the Mission-Oriented Investigation and Experimentation (MOIE) program.

This report has been reviewed by the Public Affairs Office (PAS) and is releasable to the National Technical Information Service (NTIS). At NTIS, it will be available to the general public, including foreign nationals.

This technical report has been reviewed and is approved for publication. Publication of this report does not constitute Air Force approval of the report's findings or conclusions. It is published only for the exchange and stimulation of ideas.



Carl Baner, Lt, USAF  
Project Officer



Joseph Hess, GM-15, Director West Coast  
Office, AF Space Technology Center

UNCLASSIFIED

SECURITY CLASSIFICATION OF THIS PAGE (When Data Entered)

REPORT DOCUMENTATION PAGE		READ INSTRUCTIONS BEFORE COMPLETING FORM
1. REPORT NUMBER SD-TR-85-03	2. GOVT ACCESSION NO. <b>AD A154 728</b>	3. RECIPIENT'S CATALOG NUMBER
4. TITLE (and Subtitle) Application of a Resistance Heater to the MOCVD Growth of Undoped and Se-Doped GaAs		5. TYPE OF REPORT & PERIOD COVERED
		6. PERFORMING ORG. REPORT NUMBER TR-0084A(5925-01)-1 ✓
7. AUTHOR(s) S. I. Boldish, J. S. Ciofalo, and J. P. Wendt		8. CONTRACT OR GRANT NUMBER(s) F04701-83-C-0084
9. PERFORMING ORGANIZATION NAME AND ADDRESS The Aerospace Corporation El Segundo, CA 90245		10. PROGRAM ELEMENT, PROJECT, TASK AREA & WORK UNIT NUMBERS
11. CONTROLLING OFFICE NAME AND ADDRESS Space Division Los Angeles Air Force Station Los Angeles, CA 90009-2960		12. REPORT DATE 8 March 1985
		13. NUMBER OF PAGES 12
14. MONITORING AGENCY NAME & ADDRESS (if different from Controlling Office)		15. SECURITY CLASS. (of this report) Unclassified
		15a. DECLASSIFICATION/DOWNGRADING SCHEDULE
16. DISTRIBUTION STATEMENT (of this Report)  Approved for public release; distribution unlimited.		
17. DISTRIBUTION STATEMENT (of the abstract entered in Block 20, if different from Report)		
18. SUPPLEMENTARY NOTES		
19. KEY WORDS (Continue on reverse side if necessary and identify by block number) Electrical properties, Metal-organic chemical vapor deposition, Epitaxial growth, MOCVD, GaAs, Organometallic vapor phase epitaxy, Heater design, OMVPE.		
20. ABSTRACT (Continue on reverse side if necessary and identify by block number) Described is the quartz-envelope (quartz glass outer jacket) heater, a new type of resistance heater for metal-organic chemical vapor deposition (MOCVD) systems capable of heating substrates to between 600 and 800°C. Results of epitaxial growth and electrical characterization of undoped and Se-doped GaAs from trimethylgallium and arsine are presented. Heater design and application to MOCVD growth of GaAs are detailed. The GaAs epitaxial layers were electrically characterized by Hall effect and Miller profiler.		

DD FORM 1473  
(FACSIMILE)

UNCLASSIFIED

SECURITY CLASSIFICATION OF THIS PAGE (When Data Entered)

UNCLASSIFIED

SECURITY CLASSIFICATION OF THIS PAGE(When Data Entered)

19. KEY WORDS (Continued)

20. ABSTRACT (Continued)

measurements. The best undoped GaAs has a free carrier concentration of  $3 \times 10^{14}/\text{cm}^3$  and an associated 77 K mobility of  $55\,000\text{ cm}^2\text{ V}^{-1}\text{ s}^{-1}$ ; GaAs doped with Se to  $2 \times 10^{17}/\text{cm}^3$  has a typical room-temperature mobility of  $4500\text{ cm}^2\text{ V}^{-1}\text{ s}^{-1}$ . Mobility-versus-free-carrier-concentration curves for Se-doped GaAs prepared with the quartz-envelope heater and doped GaAs grown by various MOCVD, vapor-phase epitaxy, and liquid-phase epitaxy techniques indicate the comparable or superior mobilities of material grown with the quartz-envelope heater.

UNCLASSIFIED

SECURITY CLASSIFICATION OF THIS PAGE(When Data Entered)

# PREFACE

We express our appreciation to A. B. Chase for his suggestion to use a resistance heater in an MOCVD system, and to D. H. Barker for his assistance in building and designing the first heater.

Accession For	
NTIS GRA&I	<input checked="" type="checkbox"/>
DTIC TAB	<input type="checkbox"/>
Unannounced	<input type="checkbox"/>
Justification	
By	
Distribution/	
Availability Codes	
Dist	Avail and/or Special
A-1	



## FIGURES

1.	Schematic of quartz-envelope heater, and resistance heater.....	6
2.	Thermal profiles of BN core-heater top and Si disk heated by quartz-envelope heater under various experimental conditions.....	8
3.	Background carrier concentration as a function of AsH <sub>3</sub> :TMG ratio for undoped GaAs; and as a function of growth temperature for undoped GaAs.....	10
4.	(N <sub>D</sub> - N <sub>A</sub> ) as a function of 15-ppm flow of H <sub>2</sub> Se in H <sub>2</sub> .....	11
5.	Comparison of mobility with (N <sub>D</sub> - N <sub>A</sub> ) data for Se-doped GaAs produced with quartz-envelope heater and data obtained by other techniques.....	13



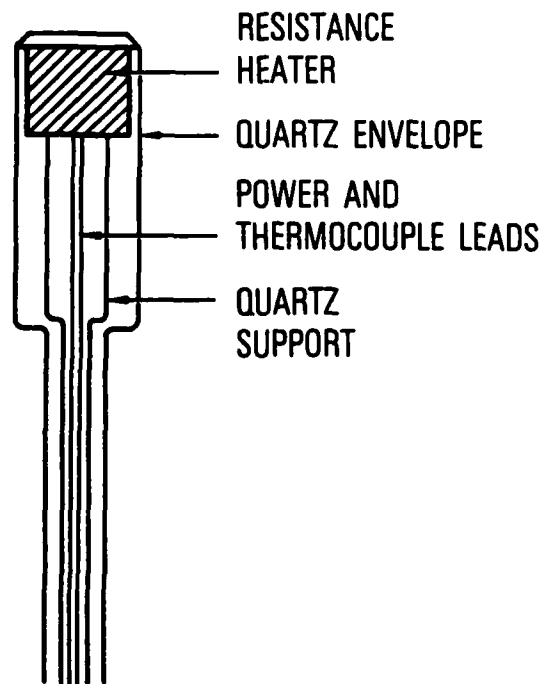
A new type of heater, the quartz-envelope heater, has been developed and used to grow undoped and Se-doped epitaxial layers of GaAs from trimethylgallium (TMG) and arsine ( $\text{AsH}_3$ ) by metal-organic chemical vapor deposition (MOCVD). The epitaxial layers are equal or superior in quality to GaAs grown by MOCVD using rf power together with a SiC-coated graphite susceptor to heat substrates to reaction temperatures ( $600\text{--}800^\circ\text{C}$ ). This report describes the construction of the heater, its application to MOCVD growth of GaAs, and the electrical properties of the epitaxial layers.

The heater (Fig. 1a) consists of a quartz envelope that houses a resistance heater (Fig. 1b) mounted on a quartz support. The resistance heater's base contains a thermocouple to measure the heater's temperature. The envelope shields the heater's functional parts from the process gases and maintains the purity of the process. Power and thermocouple leads exit the heater through the quartz support, and nitrogen constantly purges the heater through the opening in the base of the quartz-envelope heater. The heater is attached to the base of the reaction chamber with a double O-ring seal. At present, the heater is stationary during experiments, but rotation is easily implemented.

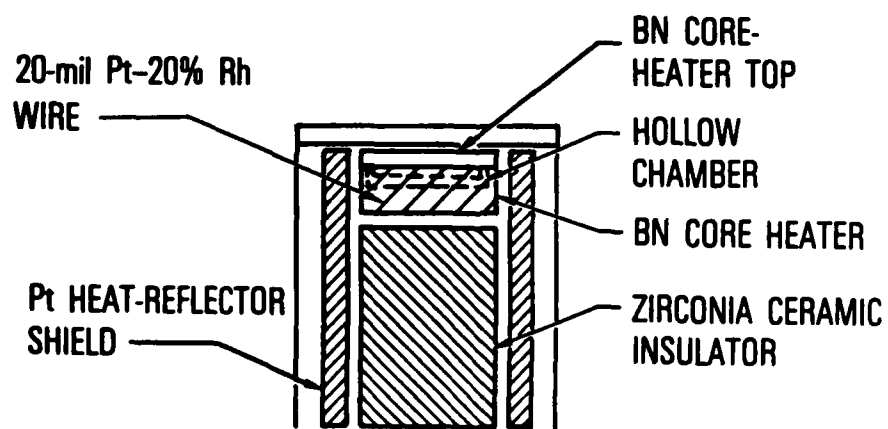
The resistance heater consists of a boron nitride (BN) core heater with zirconia ceramic insulation and a platinum heat reflector shield (Fig. 1b). The design of the heater minimizes heat dissipation through the sides of the quartz heater but maximizes heat transfer to the top plate. Consequently, the substrate is heated efficiently.

The BN core heater is shaped like a pill box to flatten the temperature profile across the substrate. The bottom is hollowed out and wrapped with 20-mil Pt—20% Rh wire, so that heat is efficiently conducted to the perimeter of the core-heater top, where heat losses are greatest. The interior surface of the top is convectively heated by  $\text{N}_2$  contained in the core-heater chamber. Temperature was regulated by a Barber Coleman 560 three-mode proportional controller and a Rubicon power controller.

Surface temperature of the heater and GaAs substrates was monitored with an Ircon infrared radiation pyrometer and a Si disk placed directly on the



(a)



(b)

Fig. 1. Schematic of (a) quartz-envelope heater, and (b) resistance heater.

heater. The disk served as a thermo-optical reference for the pyrometer so that accurate temperature measurements could be obtained. The GaAs substrate could not be used as a thermo-optical reference, because it is transparent to the 2- to 2.6- $\mu$ m light measured by the pyrometer and its emittance varies with temperature to about 800°C.

The Si disk and BN core-heater top were thermally profiled with the Ircon pyrometer (Fig. 2). The Ircon has a 75-mil lateral optical resolution. Thermal profiles of the Si disk were made in air, vacuum, and 5 standard liters per minute (SLPM) of flowing H<sub>2</sub>. The BN core-heater top was profiled only while the heater was in flowing H<sub>2</sub>. Because the results for the Si disk in air and in vacuum are identical, only results in air are presented. Flow of H<sub>2</sub> causes the thermal profile of the core-heater top to increase linearly from left to right, with a total increase of almost 15°C; the Si disk has a parabolic temperature profile, the left side being 5°C cooler than the right side. The heater is not rotated; consequently, the thermal asymmetry of the profile reflects the hydrodynamic asymmetry of the H<sub>2</sub> in the reactor chamber as it flows past the heater. The thermal-profile parabolicity of the disk results from the cooling effects of the flowing H<sub>2</sub>. Heating in air or vacuum flattens it considerably.

The carrier concentration and mobilities of the epitaxial layers were determined at room temperature and liquid-nitrogen temperature (77 K) by the van der Pauw technique<sup>1</sup> for measuring resistivity and Hall effect; room-temperature depth profiling of carrier concentrations was measured with a Leighton Miller profiler and a Hg probe.<sup>2</sup> Epitaxial-layer thickness was determined with an AB stain etch and by gravimetric methods. Hall-effect and Miller profiler carrier-concentration data did not agree for any of the undoped GaAs samples but did for some of the Se-doped material. The disagreement between carrier concentration values obtained by the two techniques can be attributed to a depletion layer that extends from the substrate--epitaxial-layer interface into the substrate.<sup>3</sup> Subtracting the width of that layer from the epitaxial-layer thickness yields an effective thickness that makes the Hall data and profile data equal.

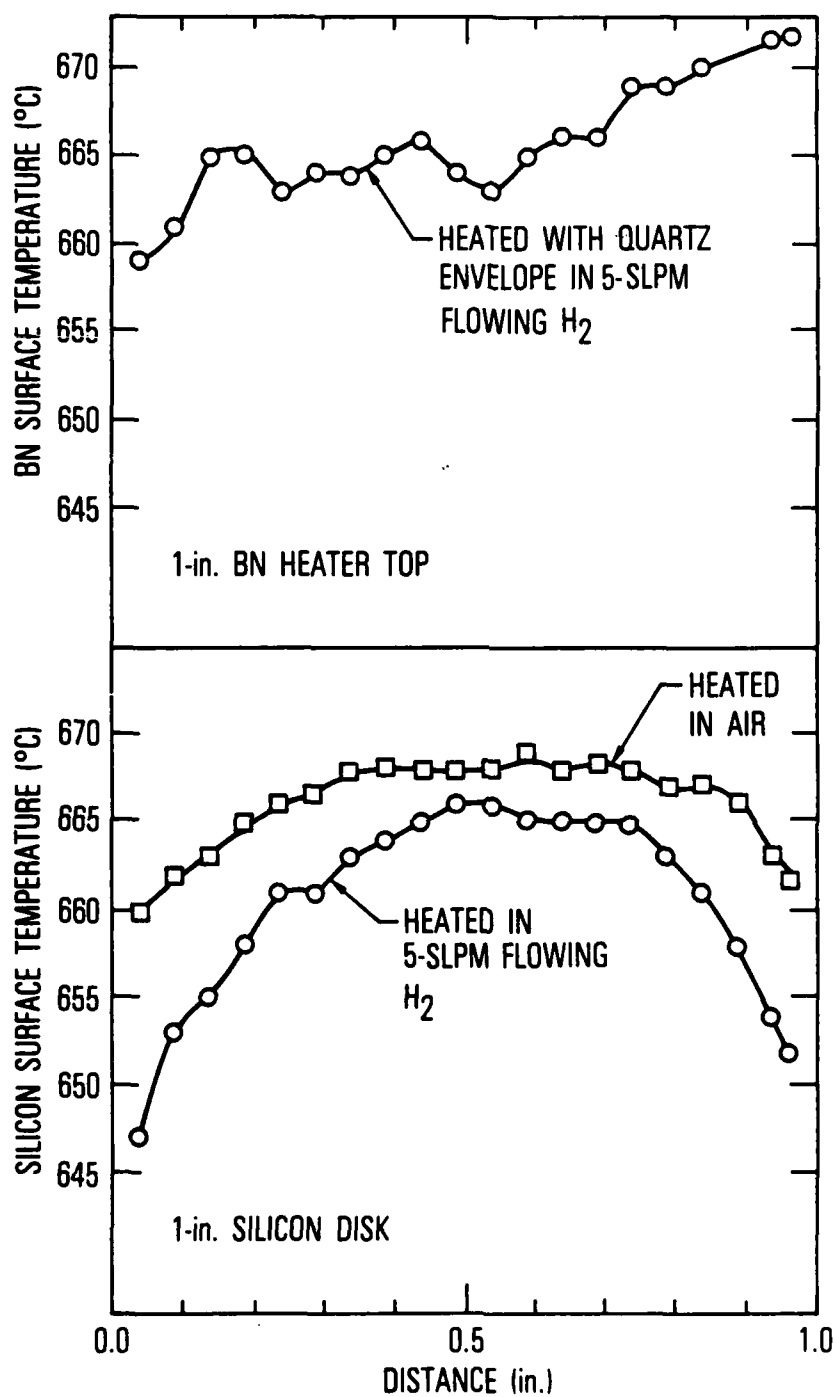


Fig. 2. Thermal profiles of BN core-heater top and Si disk heated by quartz-envelope heater under various experimental conditions.

For undoped GaAs, the typical two-winged curve is obtained for the background carrier concentration when the  $\text{AsH}_3$ :TMG ratio is varied (Fig. 3a).<sup>4</sup> An  $\text{AsH}_3$ -deficient branch is formed to the left for p-type material; an  $\text{AsH}_3$ -rich branch is formed to the right, denoting n-type material. The transition from p to n type occurs at an  $\text{AsH}_3$ :TMG ratio of almost 3.5:1. The  $\text{AsH}_3$ :TMG p-to-n transition ratio is rather small and is probably due to impurities in the  $\text{AsH}_3$  source. We have made no provisions to eliminate contaminants from the  $\text{AsH}_3$  source.

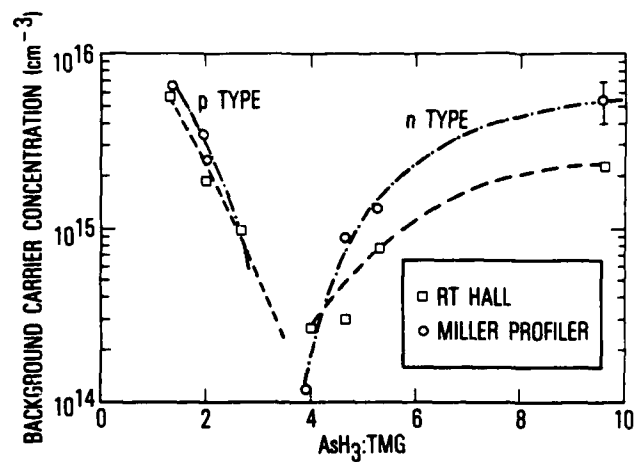
Figure 3b illustrates the increase of background carrier concentration with increasing growth temperature. The 77 K mobility reaches a maximum value of approximately  $55\,000\text{ cm}^2\text{ V}^{-1}\text{ s}^{-1}$  at a growth temperature between 630 and 650°C, but decreases markedly at both higher and lower temperatures. Data similar to those presented here were presented previously by Dapkus et al.<sup>4</sup> for a system that used rf heating and a SiC susceptor.

GaAs doping was achieved with a 15-ppm  $\text{H}_2\text{Se}$  in  $\text{H}_2$  source. The data in Fig. 4 show Se incorporation to be nonlinear with high  $\text{H}_2\text{Se}$  concentrations in the gas mixture. Similar results have been presented by Mori and Watanabe,<sup>5</sup> who indicate that, at low doping, the dopant incorporation is nearly linear with the concentration of  $\text{H}_2\text{Se}$ , whereas for high doping ( $> 10^{18}/\text{cm}^3$ ), incorporation is nonlinear with  $\text{H}_2\text{Se}$  concentration.

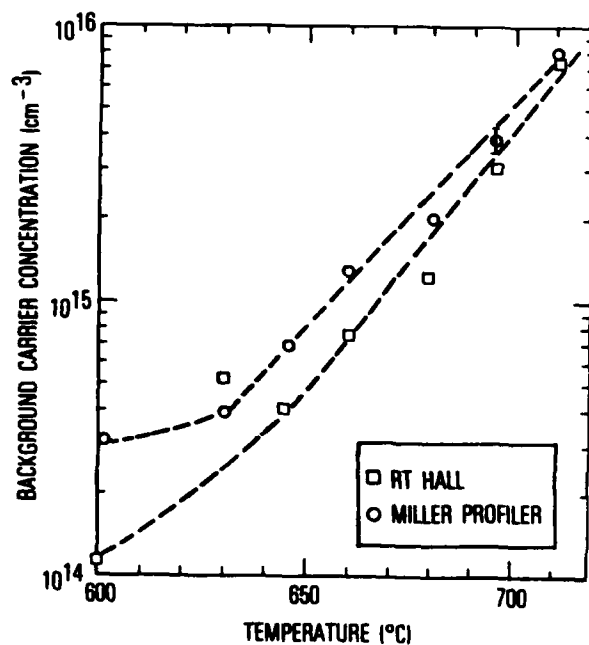
The variation of dopant incorporation with  $\text{AsH}_3$ :TMG ratio shows the same trend presented by Mori and Watanabe.<sup>5</sup> Incorporation of Se is blocked by increasing the  $\text{AsH}_3$  concentration. The effect is linear but relatively insensitive to  $\text{AsH}_3$  concentration, which appears to indicate Se has a much greater sticking coefficient than As.

Se incorporation decreases with increasing growth temperature, and an increase in growth rate increases the Se incorporation. However, Se incorporation is also relatively insensitive to these two parameters. Increased temperature can block Se incorporation by two possible mechanisms:

(1) enhanced gas-phase reaction of  $\text{H}_2\text{Se}$ , or (2) weakening the sticking coefficient of Se. The enhanced Se incorporation with increased growth rate may be caused by burying or trapping of  $\text{H}_2\text{Se}$  in the growing crystal at higher growth rates.



(a)



(b)

Fig. 3. Background carrier concentration (a) as a function of  $\text{AsH}_3:\text{TMG}$  ratio for undoped GaAs ( $T = 660^{\circ}\text{C}$ ,  $\text{TMG} = 120 \text{ SCCM}$ ); and (b) as a function of growth temperature for undoped GaAs ( $\text{TMG} = 120 \text{ SCCM}$ ; 10%  $\text{AsH}_3$  in  $\text{H}_2 = 200 \text{ SCCM}$ ; total flow = 5 SLPM).

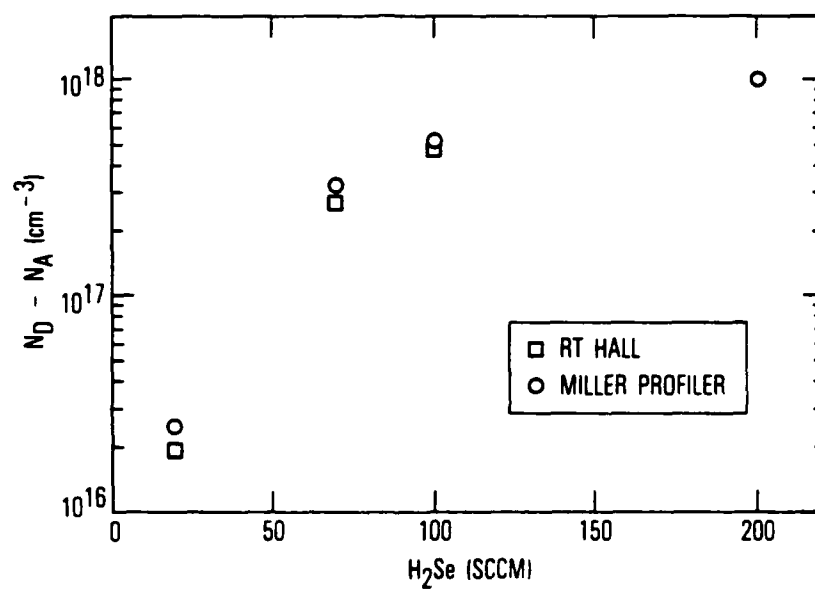


Fig. 4. ( $N_D - N_A$ ) as a function of 15-ppm flow of  $H_2Se$  in  $H_2$ .  $T = 660^\circ C$ ; TMG = 120 SCCM; 10%  $AsH_3$  in  $H_2$  = 200 SCCM; total flow = 5 SLPM.

A plot of mobility as a function of  $(N_D - N_A)$  (Fig. 5) for the Se-doped samples shows that mobility is not degraded by the use of a quartz-envelope heater. Figure 5 compares data obtained using the quartz-envelope heater with those presented by Stringfellow<sup>6</sup> and Sze and Irvin<sup>7</sup> for GaAs. The dashed curve (mobility versus impurity concentration) is more representative of the data presented here and is a valid comparison since  $(N_D - N_A) \approx (N_D + N_A)$  except at low doping levels ( $\approx 10^{16}/\text{cm}^3$ ), where  $N_D$  is not much greater than  $N_A$ .

The present heater has several limitations that can be eliminated easily: (1) it cannot rotate, (2) it can heat only 0.6 x 0.6-in. samples, and (3) it is expensive because precious metals, Pt and Rh, were used in construction. A new heater is now being constructed that will rotate and heat a 2-in.-diam wafer. Heaters have already been constructed and successfully tested with Mo and W wire in place of Pt--20% Rh.

The heater is ideally suited for an MOCVD production system, and one such system can be equipped with multiple quartz-envelope heaters. In addition to growing GaAs, the quartz-envelope heater may be employed for other types of MOCVD growth, such as that of other III-V and II-VI compounds or other single-temperature CVD processes.

In summary, the quartz-envelope heater is superior to rf and quartz halogen lamp heating because it is simple and inexpensive to construct, can be adapted readily to an MOCVD system, is capable of being thermally monitored and regulated, and can be incorporated into an MOCVD production system for growing layered structures.



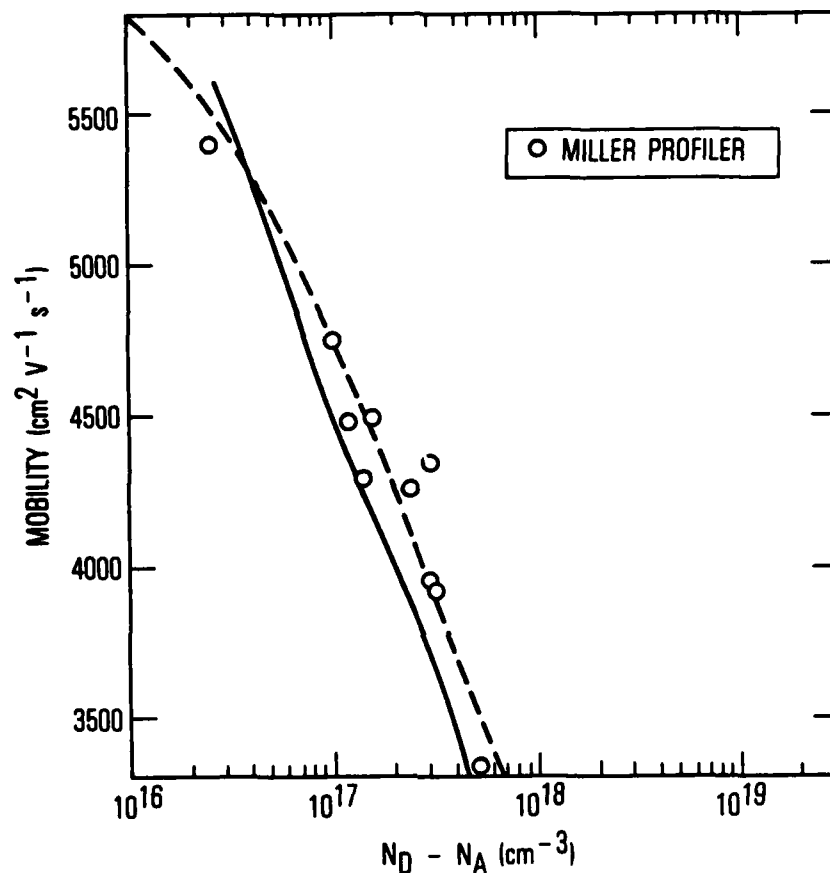


Fig. 5. Comparison of mobility with  $(N_D - N_A)$  data for Se-doped GaAs produced with quartz-envelope heater and data obtained by other techniques. Solid line is empirical representation of mobility versus  $(N_D - N_A)$  for epitaxial GaAs grown by various liquid-phase epitaxy and chemical vapor deposition techniques (including MOCVD) (Ref. 6); dashed line is empirical representation of mobility versus total impurity concentration for bulk GaAs (Ref. 7).

#### REFERENCES

1. van der Pauw, L. J., Philips Res. Rep. 13, 1 (1958).
2. Binet, M., Electron. Lett. 11, 580 (1975).
3. Boldish, S. I., J. S. Ciofalo, J. P. Wendt, submitted to J. Electron. Mater.
4. Dapkus, P. D., H. M. Manasevit, K. L. Hess, T. S. Low, and G. E. Stillman, J. Cryst. Growth 55, 10 (1981).
5. Mori, Y., and N. Watanabe, J. Appl. Phys. 52(4), 2792 (1981).
6. Stringfellow, G. B., J. Appl. Phys. 50, 4178 (1979).
7. Sze, S. M., and J. C. Irvin, Solid State Electron. 11, 599 (1968).

## LABORATORY OPERATIONS

The Laboratory Operations of The Aerospace Corporation is conducting experimental and theoretical investigations necessary for the evaluation and application of scientific advances to new military space systems. Versatility and flexibility have been developed to a high degree by the laboratory personnel in dealing with the many problems encountered in the nation's rapidly developing space systems. Expertise in the latest scientific developments is vital to the accomplishment of tasks related to these problems. The laboratories that contribute to this research are:

Aerophysics Laboratory: Launch vehicle and reentry fluid mechanics, heat transfer and flight dynamics; chemical and electric propulsion, propellant chemistry, environmental hazards, trace detection; spacecraft structural mechanics, contamination, thermal and structural control; high temperature thermomechanics, gas kinetics and radiation; cw and pulsed laser development including chemical kinetics, spectroscopy, optical resonators, beam control, atmospheric propagation, laser effects and countermeasures.

Chemistry and Physics Laboratory: Atmospheric chemical reactions, atmospheric optics, light scattering, state-specific chemical reactions and radiation transport in rocket plumes, applied laser spectroscopy, laser chemistry, laser optoelectronics, solar cell physics, battery electrochemistry, space vacuum and radiation effects on materials, lubrication and surface phenomena, thermionic emission, photosensitive materials and detectors, atomic frequency standards, and environmental chemistry.

Electronics Research Laboratory: Microelectronics, GaAs low noise and power devices, semiconductor lasers, electromagnetic and optical propagation phenomena, quantum electronics, laser communications, lidar, and electro-optics; communication sciences, applied electronics, semiconductor crystal and device physics, radiometric imaging; millimeter wave, microwave technology, and RF systems research.

Information Sciences Research Office: Program verification, program translation, performance-sensitive system design, distributed architectures for spaceborne computers, fault-tolerant computer systems, artificial intelligence and microelectronics applications.

Materials Sciences Laboratory: Development of new materials: metal matrix composites, polymers, and new forms of carbon; nondestructive evaluation, component failure analysis and reliability; fracture mechanics and stress corrosion; analysis and evaluation of materials at cryogenic and elevated temperatures as well as in space and enemy-induced environments.

Space Sciences Laboratory: Magnetospheric, auroral and cosmic ray physics, wave-particle interactions, magnetospheric plasma waves; atmospheric and ionospheric physics, density and composition of the upper atmosphere, remote sensing using atmospheric radiation; solar physics, infrared astronomy, infrared signature analysis; effects of solar activity, magnetic storms and nuclear explosions on the earth's atmosphere, ionosphere and magnetosphere; effects of electromagnetic and particulate radiations on space systems; space instrumentation.

**END**

**FILMED**

7-85

**DTIC**